Ultracompact Interference Phonon Nanocapacitor for Storage and Lasing of Coherent Terahertz Lattice Waves

Haoxue Han,[1,2] Baowen Li,[3,4,5] Sebastian Volz,[1,2] and Yuriy A. Kosevich[1,2,6,*]
[1]CNRS, UPR 288 Laboratoire d'Energétique Moléculaire et Macroscopique, Combustion (EM2C), Grande Voie des Vignes, 92295 Châtenay-Malabry, France
[2]Ecole Centrale Paris, Grande Voie des Vignes, 92295 Châtenay-Malabry, France
[3]Department of Physics, Centre for Computational Science and Engineering, and Graphene Research Center, National University of Singapore, Singapore 117546, Singapore
[4]NUS Graduate School for Integrative Sciences and Engineering, National University of Singapore, Singapore 117542, Singapore
[5]Center for Phononics and Thermal Energy Science, School of Physics Science and Engineering, Tongji University, 200092 Shanghai, People's Republic of China
[6]Semenov Institute of Chemical Physics, Russian Academy of Sciences, 4 Kosygin Street, Moscow 119991, Russia
(Received 30 September 2014; published 6 April 2015)

We introduce a novel ultracompact nanocapacitor of coherent phonons formed by high-finesse interference mirrors based on atomic-scale semiconductor metamaterials. Our molecular dynamics simulations show that the nanocapacitor stores coherent monochromatic terahertz lattice waves, which can be used for phonon lasing—the emission of coherent phonons. Either one- or two-color phonon emission can be realized depending on the geometry of the nanodevice. The two-color regime of the interference phonon nanocapacitor originates from the different incidence-angle dependence of the transmission of longitudinal and transverse phonons at the respective interference antiresonances. Coherent phonon storage can be achieved by an adiabatic cooling the nanocapacitor initially thermalized at room temperature or by the pump-probe optical technique. The linewidth narrowing and the computed relative phonon participation number confirm strong phonon confinement in the ultracompact interference nanocavity by an extremely small amount of resonance defects. The emission of coherent terahertz acoustic beams from the nanocapacitor can be realized by applying a tunable reversible stress, which shifts the frequencies of the interference antiresonances.

DOI: 10.1103/PhysRevLett.114.145501 PACS numbers: 62.25.Fg, 63.20.kp, 63.22.-m

Phonons, quanta of lattice waves, having significantly shorter wavelengths than photons at the same frequency, may allow us to pursue improved resolution in tomographic, ultrasonic, and other imaging techniques using focused sound waves. In particular, the terahertz phonons that have wavelengths comparable to the lattice constants would allow us to detect microscopic subsurface structure up to the atomic scale, also in opaque materials, with a precision higher than what optical microscopes can provide. To this end, ultrahigh-frequency coherent phonon sources are urgently desired. Coherent phonon emission and lasing have been studied in semiconductor superlattices [1–5], optomechanical systems [6–8], and electromechanical resonators [9–11], as well as in a single-ion trap [12,13] and ultracold atomic gas [14]. Coherent phonon manipulations for energy transport in dynamical nanosystems have been an emerging focus of research [15]. Various functional components of nanophononic devices, such as thermal diodes [16,17], thermal transistors [18], and thermal memory [19], have been investigated theoretically and experimentally.

Conventional sources of sound waves, such as piezoelectric transducers, fail to operate efficiently above a few tens of gigahertz. Coherent phonons were released during electrons tunneling through the coupled quantum wells [4]. Similar emission was also observed in hybrid optomechanical schemes in the range of megahertz [7] and gigahertz [20] frequencies. For these systems, the need for strong optical pumping or complex actuator tuning may limit the development of phonon lasers because unavoidable compromises have to be made in the design scheme.

In this Letter, we introduce a three-dimensional (3D) interference phonon nanocapacitor based on atomic-scale semiconductor metamaterials. The nanocapacitor allows the confinement and storage of terahertz coherent phonons with an ultrahigh monochromatic quality by an adiabatic cooling of the nanodevice or by the pump-probe optical technique [2,3]. We show that the nanocavity structure, formed by two high-finesse interference phonon metamirrors (IPMs) [21–23], can efficiently store a large number of coherent nonequilibrium phonons. The nanocapacitor can emit coherent terahertz phonon beams upon application of a tunable reversible stress. Such emission can be considered as "phonon lasing." Either one- or two-color phonon lasing can be realized depending on the geometry of the nanodevice, in contrast to the usual one-color photon lasing. The achievement of the storage and emission of coherent terahertz phonons will provide an essential step towards

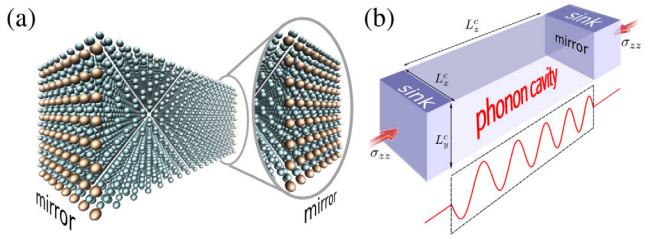

FIG. 1 (color online). Silicon phonon nanocapacitor composed of two interference phonon metamirrors separated by a spacer. (a) The atomistic view of the phonon capacitor and mirrors. The atoms in brown are Ge impurity atoms and the green ones are Si atoms of the host lattice. (b) Phonon capacitor coupled to two heat sinks under the applied uniaxial stress σ_{zz}. The dimensions of the capacitor are $L_x^c = L_y^c = 8$ nm and $L_z^c = 35$ nm.

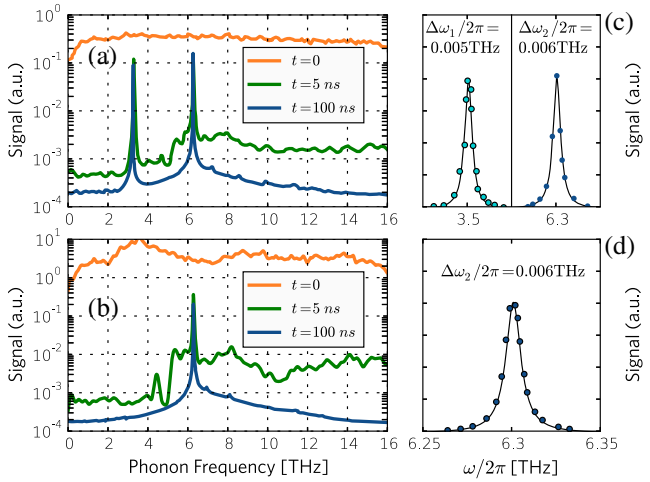

FIG. 2 (color online). Power spectral density of atomic kinetic energy in the nanocapacitor initially thermalized at $T = 300$ K as a function of time delay t after the adiabatic cooling onset. Nanocapacitor dimensions are $L_x^c = L_y^c = 8$ nm and $L_z^c = 35$ nm (a), and $L_x^c = L_y^c = 33$ nm and $L_z^c = 35$ nm (b). (c),(d) Gaussian fit of the capacitor phonon peaks to measure FWHM $\Delta\omega$ at $t = 100$ ns for the peaks in (a) and (b), respectively.

active hypersound devices and nanophononic applications of terahertz acoustics, including surgery with focused ultra- and hypersound in medicine [24]. On the other hand, the high sensitivity of the phonon interference antiresonance to the applied stresses and strains makes it possible to use the ultracompact capacitor also as a nanodetector of atomic-scale displacements and strains in the surrounding material, like a single molecule can be used as a detector of nanomechanical motion [25,26].

A detailed atomistic presentation of the phonon nanocapacitor is depicted in Fig. 1(a). The nanocapacitor consists of two parallel IPMs separated by a spacer made of bulk silicon (Si). Each IPM is composed of an atomic-scale metafilm: an internal (001) crystal plane in a cubic Si lattice partially filled with germanium (Ge) impurity atoms, as shown in Fig. 1(a). The confinement of phonon modes in the cavity results from the two-path destructive phonon interference in the metamirrors [21–23]. Ge atoms in a crystal plane of the IPM force phonons to propagate through two paths: through unperturbed (matrix) and perturbed (defect) interatomic bonds. The resulting destructive phonon interference yields transmission antiresonances (zero-transmission dips) for terahertz phonons, traversing the IPM. The random distribution of the defects in the IPM plane and the anharmonicity of atom bonds do not deteriorate the interference antiresonances [23]. Laser-assisted molecular beam epitaxy has achieved atomically sharp interfaces in a superlattice [27] and can hence provide a possible experimental implementation for the proposed nanocapacitor since this technique can reach the resolution of a single unit cell in the lattice. In the molecular dynamics (MD) simulations, we model the covalent Si:Si/Ge:Ge/Si:Ge interactions by the Stillinger-Weber potential [28]. All our MD simulations [29] were performed with the LAMMPS code package [33].

We first study the storage of coherent phonons by cooling the nanocapacitor initially thermalized at room temperature, implemented by MD simulations [29]. Two heat sinks are coupled to the capacitor on the two facets of the mirrors, as shown in Fig. 1(b). The phonons, leaving the capacitor, are dissipated once entering the sinks, which are modeled by the Langevin heat baths [34], which provide the effects of inelastic scattering on the phonon transport. The capacitor was initially thermalized homogeneously at $T = 300$ K to ensure that the material approaches the state of energy equipartition. The classical approximation remains relevant for Si at $T = 300\ \text{K} \approx 1/2\Theta_D$, where $\Theta_D = 645$ K is the Debye temperature of Si. In Figs. 2(a) and 2(b), the power spectral density of the atomic kinetic energy in the capacitor is shown, which was calculated from the windowed Fourier transform to demonstrate that all phonon modes were excited. Then, the temperature of the heat sinks was set below 40 K to cool down the capacitor [35]. In Fig. 2, the linewidth narrowing at zero temperature of the heat sinks is shown to clarify the physical mechanism. The effect of the finite temperature of the sinks is shown in Ref. [29]. In practice, liquid helium (at ~4 K) can be used for the heat sinks and Dewar flasks can be considered to prevent heat conduction and radiation from the free side surfaces in experimental implementations of the interference phonon capacitor.

We have found that the nanocapacitor can function in two regimes: in a dual-mode regime and in a single-mode regime, depending on the aspect ratio of the capacitor p defined as $p = L_x/L_z = L_y/L_z$. For a quasi-one-dimensional (quasi-1D) capacitor with a small aspect ratio $p \approx 1/4$, after $t = 5$ ns of cooling we notice the linewidth narrowing at the frequencies $\omega_1/2\pi = 3.5$ THz and $\omega_2/2\pi = 6.31$ THz, which corresponds to the dual-mode regime with the storage of both transverse and longitudinal coherent lattice waves. The power spectral density for all phonon modes in the capacitor has decayed during the

cooling process by more than 2 orders of magnitude except for the two modes, as shown in Figs. 2(a) and 2(c). With a cooling duration of $t = 100$ ns, which is very long for an atomic system, the coherent phonon peaks at $\omega_{1,2}$ show a decrease of only 10% with respect to that at $t = 5$ ns while all the other phonon modes have practically escaped the capacitor. This high monochromatic quality makes the interference cavity an ideal candidate for a coherent phonon source—the phonon laser [4,5,7,20].

The single-mode regime was achieved in a 3D capacitor with $p \approx 1$: after the same cooling process, only the longitudinal mode at $\omega_2/2\pi = 6.31$ THz is stored, as shown in Figs. 2(b) and 2(d). Since the capacitor phonons are in a single-mode state at low temperature of the heat sinks, the phonon number n_C and total elastic lattice energy $E_{\rm el}$ are related as $E_{\rm el} = \hbar\omega_2(n_C + \frac{1}{2})$. We thus obtain the phonon number $n_C \approx 57000$ for $E_{\rm el} = 77.8$ eV stored in the present nanocapacitor. In the limit of $n_C \gg 1$, n_C and ω_2 play, respectively, the role of the effective charge and potential of the phonon nanocapacitor. For a large phonon number $n_C \gg 1$, the classical equations of motion are valid for ensemble averaging in the semiclassical limit [36,37].

By the MD-based phonon wave-packet (WP) method [23], we computed the energy transmission coefficient $\alpha(\omega, \xi)$ for the Si:Ge interference mirror, for transverse and longitudinal waves. To compute $\alpha(\omega, \xi)$, we excited a 3D Gaussian wave packet centered at the frequency ω and wave vector $\mathbf{k}$ in reciprocal space and at $\mathbf{r}_0$ in real space, with the spatial width (coherence length) ξ. The WP generation was performed by assigning the displacement for the atom i:

$$\mathbf{u}_i = A\mathbf{e}_i(\mathbf{k})e^{i[\mathbf{k}\cdot(\mathbf{r}_i-\mathbf{r}_0)-\omega t]}e^{-[\mathbf{r}_i-\mathbf{r}_0-v_g t]^2/4\xi^2}, \qquad (1)$$

where A is the wave amplitude, $\mathbf{e}_i(\mathbf{k})$ is the phonon polarization vector, and v_g is the phonon group velocity at the WP center frequency ω. The WP energy transmission coefficient $\alpha(\omega, \xi)$ is defined as the ratio between the energy carried by the transmitted and initial wave packets, which are centered at the given phonon mode $(\omega, \mathbf{k})$ with the spatial extent ξ. It is determined by the convolution of the transmission coefficient for the plane wave $\alpha_{\rm pw}(\omega) = \alpha(\omega, \infty)$, described in Ref. [23], with a Gaussian WP in the frequency domain with the full width at half maximum (FWHM) $\Delta\omega = v_g/(2\xi)$: $\alpha(\omega, \xi) = \int_{-\omega_{\max}}^{\omega_{\max}} \alpha_{\rm pw}(\omega')e^{-[(\omega-\omega')^2/2\Delta\omega^2]}(d\omega'/\Delta\omega\sqrt{2\pi})$. We have confirmed that the phonon modes, trapped in the capacitor after the cooling, correspond to the antiresonance modes of the IPM, as shown in Figs. 3(a) and 3(b). Therefore, the capacitor phonons, initially excited by the external thermal or optical pumping, will experience linewidth narrowing during the cooling and concentrate at the transverse and longitudinal modes, with ω_1 and ω_2 eigenfrequencies, respectively, since the interference mirrors totally reflect

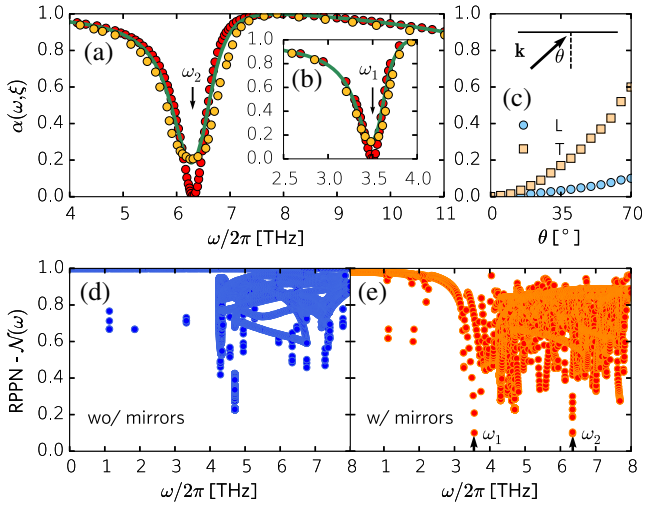

FIG. 3 (color online). (a),(b) Spectra of the energy transmission coefficient $\alpha(\omega, \xi)$ through the interference mirror obtained by MD simulations for phonon WPs with different coherence lengths ξ in Eq. (1) and incidence angles θ. Transmission of normally incident WP ($\theta = 0$) with long coherence length $\xi = 100\lambda_c$ (plane-wave approximation, red circles) and with short coherence length $\xi = 8\lambda_c$ (yellow circles) in comparison with the convolution of the plane-wave transmission spectrum $\alpha_{\rm pw}(\omega)$ with a frequency-domain Gaussian WP (green curve) with longitudinal (a) and transverse (b) polarization. (c) Transmission of the oblique-incident WP ($\theta > 0$) with $\xi = 100\lambda_c$ at the antiresonances $\omega = \omega_{1,2}$ for transverse (T) and longitudinal (L) polarizations. (d),(e) Relative phonon participation number (RPPN) $\mathcal{N}(\omega)$, Eq. (2), in a mirror-free Si sample (d) and in a capacitor formed by two IPMs (e).

the antiresonance-mode phonons but allow the other phonons to be transmitted.

The interference cavity carries out significant phonon confinement through the two-path interference in the IPMs. For a quantitative measure of phonon confinement, we introduce the relative phonon participation number $\mathcal{N}$:

$$\mathcal{N}\binom{\mathbf{k}}{\omega} = \left(\sum_{i=1}^{N}\mathcal{E}_i\binom{\mathbf{k}}{\omega}\right)^2 / N\sum_{i=1}^{N}\left[\mathcal{E}_i\binom{\mathbf{k}}{\omega}\right]^2, \qquad (2)$$

where $\mathcal{E}_i\binom{\mathbf{k}}{\omega}$, the mean kinetic energy of atom i for a normal mode $\binom{\mathbf{k}}{\omega}$ defined by the wave vector $\mathbf{k}$ and the frequency ω, can be found from the corresponding eigenvector $\epsilon_i(\mathbf{k})$, N is the total atom number in the system. $\mathcal{N} \in [0, 1]$ and measures the fraction of atoms participating in the normal vibration mode $\binom{\mathbf{k}}{\omega}$, cf. Ref. [38]. Figures 3(d) and 3(e) present a comparison between the computed $\mathcal{N}(\omega)$ in a mirror-free Si sample and in a capacitor formed by two IPMs. Most of the modes in the spectral range $\omega/2\pi \in [0, 8]$ THz are propagative since $\mathcal{N} \gtrsim 0.5$ is characteristic for the typical extended phonon modes in a perfect crystal [38]. But in the sample with the two atomic-scale

interference metamirrors, confined modes with very low $\mathcal{N}(\omega)$ (<0.1) are observed at $\omega_1/2\pi = 3.51$ THz and $\omega_2/2\pi = 6.3$ THz, which correspond exactly to the transverse and longitudinal antiresonance frequencies of the mirrors. These plots demonstrate the strong effect of an extremely small amount of Ge atoms, ~0.7%, on the phonon confinement and explain the origin of the ultracompactness of the proposed interference phonon cavity. We note that $\mathcal{N}(\frac{\mathbf{k}}{\omega})$ also describes phonon correlations in the system: it is the frequency-domain classical counterpart of the inverse time-domain second order phonon-phonon correlation function $1/g^{(2)}_{\mathrm{ph}} = \langle b^\dagger b\rangle^2/\langle b^\dagger b^\dagger bb\rangle$ [39,40], where $b^\dagger$ and b are the creation and annihilation operators of the vibrational modes, in the quantum-mechanical description of phonon confinement and correlations in the considered interference cavity.

The two-color regime of the capacitor originates from the different incidence-angle θ dependence of the transmission coefficient $\alpha(\omega, \xi, \theta)$ for the transverse and longitudinal phonons at their respective antiresonances $\omega = \omega_1, \omega_2$, as shown in Fig. 3(c). By modeling the oblique incidence of the plane-wave phonon (WP with $\xi = 100\lambda_c$), we found that $\alpha_T(\omega_2, \xi, \theta) > \alpha_L(\omega_1, \xi, \theta)$ for $\theta > 0$, showing that the oblique-incident transverse phonon has a higher transmittance through the mirror than the longitudinal counterpart. Therefore, in a 3D nanocapacitor with $p \approx 1$, IPMs are more transparent for transverse phonons among all the phonons, incident at large angles θ. Hence, only the longitudinal phonon modes remain in the capacitor after the cooling process, see Figs. 2(b) and 2(d). By contrast, in a nanocapacitor with a small aspect ratio $p \ll 1$, when the system is quasi-1D and phonons are incident upon IPMs almost normally (with θ close to 0), both the longitudinal and transverse modes are confined in the nanocapacitor [41], see Figs. 2(a) and 2(c). The two-color operation may pave the way for the dual-mode single phonon source, which is of crucial potential interest for quantum computing with phonons [42–44].

The confining effect of acoustic modes could also be found in a subterahertz acoustic nanocavity [1,2] placed between two Bragg reflectors (BRs). The nanocavity mode corresponds to the Fabry-Pérot resonance in the inhibited band gap background of the surrounding BRs [1,3]. Such a Fabry-Pérot mode gives rise to the total transmission peak lying inside the wide phonon band gap, which can be identified as "resonance tunneling." The interference phonon cavity has several differences from the acoustic cavity placed between two BRs [29], and the important advantage is related to the fact that BRs are made of several periods of the semiconductor superlattice with a total thickness of several dozen nanometers [1–3], while IPMs in the interference phonon cavity require only single-atom crystal planes, which enables the potential realization of ultracompact nanophononic devices.

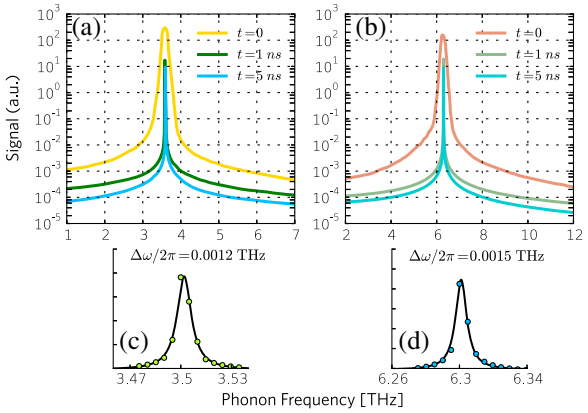

FIG. 4 (color online). Power spectral density of atomic kinetic energy in the capacitor after excitation of the transverse (a) and longitudinal (b) phonon WP as a function of time delay t. The peaks centered at $\omega_{1,2}$ demonstrate a continuous linewidth narrowing as a function of t. At $t = 5$ ns, the widths narrow down to $\Delta\omega_1/2\pi = 1.2 \times 10^{-3}$ THz and $\Delta\omega_2/2\pi = 1.5 \times 10^{-3}$ THz, which correspond to the cavity Q factors of $Q_1 = 2916$ and $Q_2 = 4208$, respectively. Gaussian fit of the capacitor phonon peaks to measure FWHM $\Delta\omega$ at $t = 5$ ns for the transverse (c) and longitudinal (d) modes.

To understand better the generation mechanism of the capacitor phonons, we have studied the evolution of lattice dynamics in the nanocapacitor after its excitation in the form of a phonon WP (see also Ref. [29]). We demonstrate through the mapping of the power spectral density of the atomic kinetic energy in the capacitor, shown in Fig. 4, that the Gaussian phonon WP, initially centered at $(\omega, \mathbf{k})$, finally transforms into coherent monochromatic standing wave composed of the two plane waves with the same frequency ω and opposite wave vectors $\pm\mathbf{k}$ along the normal to the mirrors (when $\xi \gg L_z^c$). Between the free side surfaces of the capacitor, a standing wave with the wavelength $\lambda = 2L_x^c$ of the sinusoidal envelope is formed. In practice, the pump-probe optical technique [2,3] can be used to excite the capacitor phonons, and the considered WP excitation mimics this technique.

We now turn to the controllable emission of the coherent phonons from the capacitor. Figure 5 shows the shift of the interference antiresonance spectral loci for transverse and longitudinal phonons caused by the uniaxial stress σ_{zz}, applied in the [001] direction to the interference cavity as shown in Fig. 1(b). The resulting strain ϵ produces the change in the local force constants between the Ge and Si atoms in the mirrors, which shifts the antiresonance frequencies $\omega_{1,2}$ of the capacitor, according to the value of the Grüneisen parameter of Si. Through such a mechanism, we are able to emit coherent phonons by applying a tunable reversible uniaxial stress at the tips of the device [45] (and the resulting strain can be rather small, $\epsilon = 1\%$, see Ref. [29]). Once the external stress is released, the phonon emission is switched off due to the recovery of the

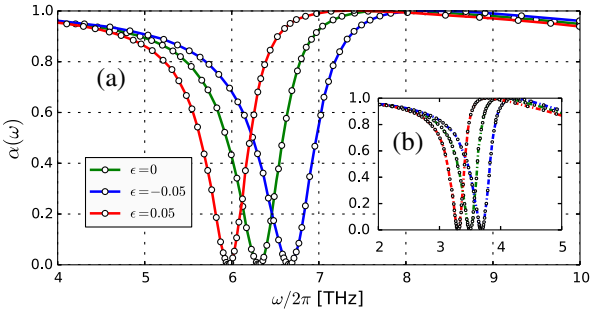

FIG. 5 (color online). Shift of the interference antiresonance spectral loci caused by a tunable strain ϵ in the capacitor. Antiresonance frequency shifts for longitudinal (a) and transverse (b) plane waves, normally incident on the interference mirror. Interference cavity is exposed to the uniaxial strain ϵ in the $\langle 001 \rangle$ direction.

interference metamirrors back to the original antiresonance frequencies. Therefore, the directional and coherent phonon emission from the interference cavity, which can be considered as phonon lasing [10,13], is flexibly switched by the external stress. The two- or three-color phonon lasing of both longitudinal and transverse coherent lattice waves can be realized from the quasi-1D nanocapacitor [41].

The interference phonon capacitor may be a new component for constructing and controlling macroscopic artificial quantum systems based on sound. The tunable strain-engineered discharging of the nanocapacitor and the two- or three-color phonon emission may also be relevant for quantum computing with phonons: to inhibit decoherence and to yield single phonons. Moreover, phonons from the nanocapacitor can be coupled to optical fields and an electronic subsystem, which enables the ultracompact interference phonon capacitor to play an important potential role in a hybrid quantum computing architecture [42–44].

*Corresponding author.
yukosevich@gmail.com

[1] M. Trigo, A. Bruchhausen, A. Fainstein, B. Jusserand, and V. Thierry-Mieg, Phys. Rev. Lett. **89**, 227402 (2002).
[2] A. Huynh, N. D. Lanzillotti-Kimura, B. Jusserand, B. Perrin, A. Fainstein, M. F. Pascual-Winter, E. Peronne, and A. Lemaître, Phys. Rev. Lett. **97**, 115502 (2006).
[3] N. D. Lanzillotti-Kimura, A. Fainstein, A. Huynh, B. Perrin, B. Jusserand, A. Miard, and A. Lemaître, Phys. Rev. Lett. **99**, 217405 (2007).
[4] R. P. Beardsley, A. V. Akimov, M. Henini, and A. J. Kent, Phys. Rev. Lett. **104**, 085501 (2010).
[5] W. Maryam, A. V. Akimov, R. P. Campion, and A. J. Kent, Nat. Commun. **4**, 2184 (2013).
[6] T. J. Kippenberg and K. J. Vahala, Science **321**, 1172 (2008).
[7] I. S. Grudinin, H. Lee, O. Painter, and K. J. Vahala, Phys. Rev. Lett. **104**, 083901 (2010).
[8] J. B. Khurgin, M. W. Pruessner, T. H. Stievater, and W. S. Rabinovich, Phys. Rev. Lett. **108**, 223904 (2012).
[9] I. Mahboob, K. Nishiguchi, H. Okamoto, and H. Yamaguchi, Nat. Phys. **8**, 387 (2012).
[10] I. Mahboob, K. Nishiguchi, A. Fujiwara, and H. Yamaguchi, Phys. Rev. Lett. **110**, 127202 (2013).
[11] H. Okamoto, A. Gourgout, C.-Y. Chang, K. Onomitsu, I. Mahboob, E. Y. Chang, and H. Yamaguchi, Nat. Phys. **9**, 480 (2013).
[12] A. E. Kaplan, Opt. Express **17**, 10035 (2009).
[13] K. Vahala, M. Herrmann, S. Knünz, V. Batteiger, G. Saathoff, T. W. Hänsch, and Th. Udem, Nat. Phys. **5**, 682 (2009).
[14] J. T. Mendonça, H. Terças, G. Brodin, and M. Marklund, Europhys. Lett. **91**, 33001 (2010).
[15] N. Li, J. Ren, L. Wang, G. Zhang, P. Hänggi, and B. Li, Rev. Mod. Phys. **84**, 1045 (2012).
[16] B. Li, L. Wang, and G. Casati, Phys. Rev. Lett. **93**, 184301 (2004).
[17] C. W. Chang, D. Okawa, A. Majumdar, and A. Zettl, Science **314**, 1121 (2006).
[18] B. Li, L. Wang, and G. Casati, Appl. Phys. Lett. **88**, 143501 (2006).
[19] R. Xie, C. Bui, B. Varghese, Q. Zhang, C. Sow, B. Li, and J. Thong, Adv. Funct. Mater. **21**, 1602 (2011).
[20] A. Fainstein, N. D. Lanzillotti-Kimura, B. Jusserand, and B. Perrin, Phys. Rev. Lett. **110**, 037403 (2013).
[21] Yu. A. Kosevich, Prog. Surf. Sci. **55**, 1 (1997).
[22] Yu. A. Kosevich, Phys. Usp. **51**, 848 (2008).
[23] H. Han, L. G. Potyomina, A. A. Darinskii, S. Volz, and Yu. A. Kosevich, Phys. Rev. B **89**, 180301(R) (2014).
[24] T. D. Khokhlova, Y.-N. Wang, J. C. Simon, B. W. Cunitz, F. Starr, M. Paun, L. A. Crum, M. R. Bailey, and V. A. Khokhlova, Proc. Natl. Acad. Sci. U.S.A. **111**, 8161 (2014).
[25] V. Puller, B. Lounis, and F. Pistolesi, Phys. Rev. Lett. **110**, 125501 (2013).
[26] Y. Tian, P. Navarro, and M. Orrit, Phys. Rev. Lett. **113**, 135505 (2014).
[27] J. Ravichandran *et al.*, Nat. Mater. **13**, 168 (2014).
[28] F. H. Stillinger and T. A. Weber, Phys. Rev. B **31**, 5262 (1985).
[29] See Supplemental Material at http://link.aps.org/supplemental/10.1103/PhysRevLett.114.145501, which includes Refs. [30–32], for the details of the simulation setup, dynamical evolution of the phonon wave packet, and linewidth narrowing in the interference nanocavity coupled to heat sinks with finite temperature.
[30] A. Bodapati, P. K. Schelling, S. R. Phillpot, and P. Keblinski, Phys. Rev. B **74**, 245207 (2006).
[31] L. Yang, N. Yang, and B. Li, Nano Lett. **14**, 1734 (2014).
[32] S. Pailhès, H. Euchner, V. M. Giordano, R. Debord, A. Assy, S. Gomès, A. Bosak, D. Machon, S. Paschen, and M. de Boissieu, Phys. Rev. Lett. **113**, 025506 (2014).
[33] S. J. Plimpton, Comput. Phys. **117**, 1 (1995).
[34] F. Bonetto, J. L. Lebowitz, and L. Rey-Bellet, in *Mathematical physics 2000*, edited by A. Fokas, A. Grigoryan, T. Kibble, and B. Zegarlinski (Imperial College Press, London, 2000), pp. 128–150.
[35] The switch on of the heat sinks takes only a few picoseconds, during which the phonons present in the capacitor have no time to escape, which corresponds to an "adiabatic cooling" process.
[36] C. W. Gardiner and P. Zoller, *Quantum noise* (Springer, Berlin, 2004).

[37] M. Aspelmeyer, T. J. Kippenberg, and F. Marquardt, Rev. Mod. Phys. **86**, 1391 (2014).
[38] R. J. Bell and P. Dean, Discuss. Faraday Soc. **50**, 55 (1970).
[39] J. Kabuss, A. Carmele, T. Brandes, and A. Knorr, Phys. Rev. Lett. **109**, 054301 (2012).
[40] K. V. Kepesidis, S. D. Bennett, S. Portolan, M. D. Lukin, and P. Rabl, Phys. Rev. B **88**, 064105 (2013).
[41] If the defect-filled crystal planes of IPMs have lower symmetry, e.g., coincide with (110) crystal planes in the cubic Si lattice, the quasi-1D capacitor will store three phonon modes, one longitudinal and two nondegenerate transverse modes, since Si and Ge single crystals are anisotropic phononic materials, see, e.g., J. J. Wortman and R. A. Evans, J. Appl. Phys. **36**, 153 (1965); A. M. Kosevich, Yu. A. Kosevich, and E. S. Syrkin, Sov. Phys. JETP **61**, 639 (1985).
[42] Ö. O. Soykal, R. Ruskov, and C. Tahan, Phys. Rev. Lett. **107**, 235502 (2011).
[43] R. Ruskov and C. Tahan, Phys. Rev. B **88**, 064308 (2013).
[44] S. Sklan and J. C. Grossman, arXiv:1301.2807.
[45] The stored coherent phonons are emitted from the capacitor with the group velocity $v_{gz}(\omega, k_z) = \partial\omega/\partial k_z$ of the phonon mode.